The “Backward Looking” Effect in the Continuum Model Considering a New Backward Equilibrium Velocity Function

Md Anowar Hossain (anowar.math.buet@gmail.com)
Kyushu University - Chikushi Campus: Kyushu Daigaku - Chikushi Campus
TANIMOTO Jun
Kyushu University - Chikushi Campus: Kyushu Daigaku - Chikushi Campus

Research Article

Keywords: Continuum traffic model, new backward equilibrium velocity function, backward-looking effect, nonlinear analysis, numerical simulation

Posted Date: May 17th, 2021

DOI: https://doi.org/10.21203/rs.3.rs-517317/v1

The "backward looking" effect in the continuum model considering a new backward equilibrium velocity function.

Authors

Md. Anowar Hossain[a)], Jun Tanimoto[a), b)]

[a)] Interdisciplinary Graduate School of Engineering Sciences, Kyushu University, Kasuga-koen, Kasuga-shi, Fukuoka, 816-8580, Japan.

[b)] Faculty of Engineering Sciences, Kyushu University, Kasuga-koen, Kasuga-shi, Fukuoka, 816-8580, Japan.

Corresponding author

Md. Anowar Hossain, anowar.math.buet@gmail.com

PACS numbers

PACS: 89.40.-a (Transportation); 87.15. Aa (Theory and modeling; Computer simulation)

Keywords

Continuum traffic model, new backward equilibrium velocity function, backward-looking effect, nonlinear analysis, numerical simulation

Highlights

- The backward-looking traffic flow model, a new continuum traffic model, is developed.
- The backward-looking effect is considered by applying a new backward equilibrium velocity function.
- Linear stability and nonlinear analyses are conducted, and the Korteweg–de Vries–Burgers equation and the attendant analytical solution are drawn.
- The numerical simulation demonstrates that the proposed model enhances traffic flow stability.

Abstract

In this paper, a new continuum traffic model is developed considering the backward-looking effect through a new positive backward equilibrium speed function. As compared with the conventional full velocity difference model, the backward equilibrium velocity function, which is largely acceptably grounded from mathematical and physical perspectives, plays an important role in significantly enhancing the stability of the traffic flow field. A linear stability condition is derived to demonstrate the flow neutralization capacity of the model, whereas the Korteweg–de Vries–Burgers equation and the attendant analytical solution are deduced using nonlinear analysis to observe the traffic flow behavior near the neutral stability condition. A numerical simulation, used to determine the flow stability enhancement efficiency of the model, is also conducted to verify the theoretical results.

1. Introduction

In recent years, mass communication complexities have emerged within urban society. Scientists, transportation engineers, and local governments have put forward various ideas and projects to overcome the problem of traffic congestion. Within this, a great number of traffic models have been proposed in relation to various phenomena, including microscopic models [1–10], continuum models [11–16], cellular automated models [17–21], and lattice hydrodynamic models [22–28].

In 1955, a new dimension was added to the traffic flow dynamics by Lighthill, Whitham, and Richard with their so-called LWR model [29–31]. In this model, the fluid flow concept is implemented within the traffic flow system using a simple first-order continuity equation, with the model known as a macroscopic model. The dynamical equation of the LWR continuum model is as follows:

$$\frac{\partial \rho}{\partial t} + \frac{\partial (\rho v)}{\partial x} = 0. \tag{1}$$

where ρ, v, x, and t are the density, velocity, space, and time, respectively, of the traffic flow system.

However, the LWR model fails to accurately explain the non-equilibrium states of a real traffic flow field. In view of overcoming this limitation, Payne [32] suggested another high-order continuum model of traffic dynamics; the mathematical expression of which is as follows:

$$\frac{\partial v}{\partial t} + v\frac{\partial v}{\partial x} = -\frac{\mu}{\rho T}\frac{\partial \rho}{\partial x} + \frac{v_e - v}{T}, \tag{2}$$

where μ is the anticipation coefficient and T is the relaxation time.

Meanwhile, in 1995, on the basis of the Lagrangian viewpoint, Bando et al. [33] proposed the optimal velocity (OV) model, a revolutionary traffic model, in which vehicles are regarded as granular dynamics of the flow field. Here, the vehicle's speed is adjusted by the OV function, which depends on the headway distance of the vehicle. This model has proven to be extremely convenient in terms of both theoretical analyses and numerical simulations since, given that all drivers have a unique sensitivity, the road is regarded as a single-lane system where overtaking is not permitted. The dynamical equation of this model is as follows:

$$\frac{dv_n(t)}{dt} = a[V[\Delta x_n(t)] - v_n(t)], \tag{3}$$

where a is the unique sensitivity of all drivers, $v_n(t)$ is the speed of the nth vehicle at time t, $V\left(\Delta x_n(t)\right)$ is the OV of the nth vehicle, and $\Delta x_n(t)$ is the headway distance of the nth vehicle, as measured in terms of $\Delta x_n(t) = x_{n+1}(t) - x_n(t)$.

The OV model has certain limitations, with the acceleration and deacceleration of the model regarded as largely unrealistic. To address this inherent defect, Helbing and Tilch [34] developed the so-called generalized force model by introducing a negative speed difference to the OV model. Meanwhile, in 2001, Jiang et al. [35] demonstrated that, in addition to the negative speed difference, the positive velocity difference also has a great impact on increasing the flow stability. As such, the full velocity difference (FVD) model was proposed, with the attendant mathematical expression as follows:

$$\frac{dv_n(t)}{dt} = a[V[\Delta x_n(t)] - v_n(t)] + \lambda \Delta v_n(t), \tag{4}$$

where $\Delta v_n(t)$ is the velocity difference between the $n+1$th and the nth car, as quantified by $\Delta v_n(t) = v_{n+1}(t) - v_n(t)$, and λ is the sensitivity coefficient independent of a.

All of these conventional models fully rely on the preceding headway gap. However, in an actual traffic flow system, the speed characteristics of the follower vehicle would also come into play. In introducing this aspect, Nakayama et al. [36] proposed the BLOV model, an effective car-following model, in which a backward OV function was established alongside the forward optimal function. Although the BLOV car-following model is largely heralded from a real-life viewpoint, the model has several crucial drawbacks in terms of formulating the backward OV function, which is defined by a negative function that is regarded as unrealistic. To overcome this drawback, various robust car-following models have been proposed [37, 38] with the incorporation of a new backward OV function as a positive function, which inevitably increases the stability of the flow field. Here, Zhaoze et al. [39] proposed a continuum traffic model based on the BLOV model, wherein the backward equilibrium speed is quantified by a negative function, which is regarded as unacceptable from a mathematical viewpoint. In the present study, a continuum traffic model is developed with consideration of a new backward equilibrium speed function. Here, the backward equilibrium speed is measured via a positive function depending on the local density, much like with the forward OV. The drawbacks of the existing models could be eliminated through the application of this function, with the stability of the flow field significantly enhanced.

The remainder of the paper is organized as follows. Section 2 describes the formulation of the proposed model, followed by a discussion on the neutral stability analysis in Section 3. Section 4 then presents the nonlinear analysis, whereas Section 5 outlines the numerical simulation and the model results. Finally, Section 6 concludes the paper with the main findings.

2. Model formulation

This continuum model is developed based on the concept of the backward-looking effect [37, 38]. The dynamical equation of the FVD model with the backward-looking effect is as follows:

$$\frac{dv_n(t)}{dt} = a[p \cdot V_F[\Delta x_n(t)] + (1-p) \cdot V_B[\Delta x_{n-1}(t)] - v_n(t)] + \lambda \cdot \Delta v_n(t), \tag{5}$$

where p is the forward concentration of drivers and V_F and V_B are the forward and backward optimal velocities, respectively.

To convert the variables from the micro to the macro, the following transform is conducted:

$$\begin{aligned}
&v_n(t) \to v(x,t),\\
&v_{n+1}(t) \to v(x+\Delta,t),\\
&\mathrm{V}_F[\Delta x_n(t)] \to \mathrm{V}_{eF}(\rho),\\
&\mathrm{V}_F'[\Delta x_n(t)] \to \overline{\mathrm{V}}_{eF}'(h) \to -\rho^2 \mathrm{V}_{eF}'(\rho),\\
&\mathrm{V}_B[\Delta x_{n-1}(t)] \to \mathrm{V}_{eB}(\rho),\\
&\mathrm{V}_B'[\Delta x_{n-1}(t)] \to \overline{\mathrm{V}}_{eB}'(h) \to \rho^2 \mathrm{V}_{eB}'(\rho),
\end{aligned} \tag{6}$$

where $v(x,t)$ and $\rho(x,t)$ are the velocity and density, respectively, in the macroscopic system; Δ is the distance between two adjacent vehicles; $h = \frac{1}{\rho}$ represents the average headway; and $V_{eF}(\rho)$ and $V_{eB}(\rho)$ are the equilibrium speed function for forward and backward, respectively.

Although considering the backward OV as a negative function of the forward OV [36, 40, 41], except for one or two outstanding works [37, 38], a great number of backward-looking car-following models have been proposed. Similarly, in designing a continuum model for the backward-looking effect, the pioneering

models regarded the backward equilibrium as a negative function of the forward equilibrium function, which is seen as unrealistic [39, 42, 43]. In our proposed model, we assume a new positive function for the backward equilibrium velocity, much like with the forward equilibrium speed. The functions of these equilibrium speeds can be defined as follows [44]:

$$\mathrm{V}_{eF}(\rho) = v_{ff}\left[\left(1+\exp\frac{\rho/\rho_m-0.25}{0.06}\right)^{-1} - 3.72\times10^{-6}\right], \tag{7}$$

$$\mathrm{V}_{eB}(\rho) = v_{bf}\left[\left(1+\exp\frac{0.25-\rho/\rho_m}{0.06}\right)^{-1} - 3.72\times10^{-6}\right], \tag{8}$$

where ρ_m is the maximum density of the flow field and v_{ff} and v_{bf} are the free-flow speed for the forward and backward equilibrium velocity functions, respectively. Generally, $v_{ff} \neq v_{bf}$; however, here, both cases were studied, that is, for $v_{ff} = v_{bf}$ and for $v_{ff} \neq v_{bf}$.

The term $v(x+\Delta, t)$ can be expanded by the Taylor series as follows:

$$v(x+\Delta, t) = v(x,t) + v_x\Delta + \frac{1}{2}v_x\Delta^2. \tag{9}$$

By substituting the macroscopic variables into Eq. (5), we could obtain the following equation:

$$\frac{\partial v}{\partial t} + (v-\lambda\Delta)\frac{\partial v}{\partial x} = a[p\mathrm{V}_{eF}(\rho) + (1-p)\mathrm{V}_{eB}(\rho) - v] + \frac{\lambda\Delta^2}{2}v_{xx}. \tag{10}$$

Meanwhile, by combining Eq. (10) and Eq. (1), we could obtain the following equations in macro form:

$$\begin{aligned} &\frac{\partial \rho}{\partial t} + \rho\frac{\partial v}{\partial x} + v\frac{\partial \rho}{\partial x} = 0, \\ &\frac{\partial v}{\partial t} + (v-\lambda\Delta)\frac{\partial v}{\partial x} = a\left[pV_{fe}(\rho) + (1-p)V_{be}(\rho) - v\right] + \frac{\lambda\Delta^2}{2}v_{xx}. \end{aligned} \tag{11}$$

This presents the mathematical expression of the continuum traffic flow model incorporating the pressure effect of backward density.

3. Linear stability analysis

Linear stability analysis is conducted to examine the flow stability of the model. The vector form of the proposed model is as follows:

$$\boldsymbol{H}t + \boldsymbol{A}\boldsymbol{H}x = \boldsymbol{E}, \tag{12}$$

where

$$\boldsymbol{H} = \begin{bmatrix}\rho\\ v\end{bmatrix}, \boldsymbol{A} = \begin{bmatrix}v & \rho\\ 0 & v-\lambda\Delta\end{bmatrix}, \tag{13}$$

$$\boldsymbol{E} = \begin{bmatrix}0\\ a\left[pV_{fe}(\rho) + (1-p)V_{be}(\rho) - v\right] + \frac{\lambda\Delta^2}{2}v_{xx}\end{bmatrix}. \tag{14}$$

The eigenvalues of $\boldsymbol{A}$ are given by the following:

$$\lambda_1 = v \text{ and } \lambda_2 = v - \lambda\Delta. \tag{15}$$

Let us consider that ρ_0 and v_0 are the density and velocity at an initial time for a homogeneous traffic flow field, respectively. Here, the steady-state solution of the continuum model can be described as follows:

$$\rho(x,t) = \rho_0,\ v(x,t) = v_0. \tag{16}$$

Applying the small perturbation to the uniform flow system, we could obtain the following solution:

$$\begin{pmatrix}\rho(x,t)\\ v(x,t)\end{pmatrix} = \begin{pmatrix}\rho_0\\ v_0\end{pmatrix} + \begin{pmatrix}\hat{\rho}_k\\ \hat{v}_k\end{pmatrix}\exp(ikx + \sigma_k t), \tag{17}$$

where k and σ_k are the number and frequency of the waves, respectively.

By substituting the perturbation solution Eq. (17) into Eq. (11), we could obtain the following equations by simplifying and neglecting the higher-order terms:

$$\begin{aligned}&(\sigma_k + v_0 ik)\hat{\rho}_k + \rho_0 ik\hat{v}_k = 0,\\ &a\left[pV_{fe}'(\rho_0) + (1-p)V_{be}'(\rho_0)\right]\hat{\rho}_k - \left[a + \frac{\lambda\Delta^2 k^2}{2} + \sigma_k + (v_0 - \lambda\Delta)ik\right]\hat{v}_k = 0.\end{aligned} \tag{18}$$

From Eq. (18), we could obtain a quadratic equation as follows :

$$\begin{aligned}&(\sigma_k + v_0 ik)^2 + \left(a + \frac{\lambda\Delta^2 k^2}{2} - ik\lambda\Delta\right)(\sigma_k + v_0 ik) + \Big(pV_{fe}'(\rho_0) + (1-\\ &\quad p)V_{be}'(\rho_0)\Big)(a\rho_0 ik) = 0.\end{aligned} \tag{19}$$

To ensure a stable flow, both roots of σ_k must have negative real parts. Thus, the traffic flow field will be stable under the following states:

$$a + \lambda\Delta + \left[p\cdot\rho_0 V_{fe}'(\rho_0) + (1-p)\cdot\rho_0 V_{be}'(\rho_0)\right] > 0. \tag{20}$$

Therefore, the final neutral stability condition could be deduced from Eq. (20) in the following form:

$$a_s = -\left(\lambda\Delta + \left[p\cdot\rho_0 V_{fe}'(\rho_0) + (1-p)\cdot\rho_0 V_{be}'(\rho_0)\right]\right). \tag{21}$$

The imaginary part of σ_k is given as follows:

$$\mathrm{Im}(\sigma_k) = -k\left(v_0 + \left[p\cdot\rho_0 V_{fe}'(\rho_0) + (1-p)\cdot\rho_0 V_{be}'(\rho_0)\right]\right) + o(k^3). \tag{22}$$

For a small disturbance, the propagation critical speed of Eq. (21) is as follows:

$$\mathrm{c}(\rho_0) = v_0 + \left[p\cdot\rho_0 V_{fe}'(\rho_0) + (1-p)\cdot\rho_0 V_{be}'(\rho_0)\right]. \tag{23}$$

Based on the neutral stability condition described by Eq. (21), Fig. 1 shows the flow stability states of the continuum model for two cases: (a) the equal ($v_{ff} = v_{bf}$) and (b) the unequal ($v_{ff} \neq v_{bf}$) free-flow speed of the forward and backward equilibrium velocity functions. The model was fully consistent with the conventional FVD model when presuming $p = 1.0$, with the flow stabilization capacity of the proposed model significantly increased compared with the conventional FVD model, as shown in Fig. 1a and Fig. 1b. In fact, as Fig. 1 shows, it was confirmed that the flow stability of our model increased with the decrease in p value and that the model performed better for $v_{ff} = v_{bf}$ than for $v_{ff} \neq v_{bf}$. It can thus be stated that the stability of the traffic flow field was substantially enhanced by the effect of the new backward equilibrium velocity function.

4. Nonlinear analysis

To discuss the nonlinear properties of the model, a nonlinear analysis is conducted. Here, to examine the system behavior near the neutral stability condition, a new coordinate system is introduced as follows [11]:

$$z = x - ct. \tag{24}$$

By combining Eq. (11) with Eq. (24), we could obtain the following equations:

$$\begin{aligned} &-c\rho_z + q_z = 0, \\ &-cv_z + (v - \lambda\Delta)v_z = a\left[pV_{fe}(\rho) + (1-p)V_{be}(\rho) - v\right] + \frac{\lambda\Delta^2}{2}v_{xx}. \end{aligned} \tag{25}$$

where the traffic flow flux is the product of density and velocity, i.e., $q = \rho.v$, with this equation deduced in terms of the following forms:

$$\begin{aligned} &v_z = \frac{c\rho_z}{\rho} - \frac{q\rho_z}{\rho^2}, \\ &v_{zz} = \frac{c\rho_{zz}}{\rho} - \frac{2c\rho_z^2}{\rho^2} - \frac{q\rho_{zz}}{\rho^2} + \frac{2q\rho_{zz}^2}{\rho^3}. \end{aligned} \tag{26}$$

By substituting Eq. (26) into Eq. (25), we could obtain the following:

$$\begin{aligned} &-c\left(\frac{c\rho_z}{\rho} - \frac{q\rho_z}{\rho^2}\right) + \left(\frac{q}{\rho} - \lambda\Delta\right)\left(\frac{c\rho_z}{\rho} - \frac{q\rho_z}{\rho^2}\right) = a\left[pV_{fe}(\rho) + (1-p)V_{be}(\rho) - \frac{q}{\rho}\right] + \\ &\frac{\lambda\Delta^2}{2}\left(\frac{c\rho_{zz}}{\rho} - \frac{2c\rho_z^2}{\rho^2} - \frac{q\rho_{zz}}{\rho^2} + \frac{q\rho_z^2}{\rho^3}\right). \end{aligned} \tag{27}$$

The flow flux q can be expressed as follows:

$$q = \rho\left[pV_{fe}(\rho) + (1-p)V_{be}(\rho)\right] + b_1\rho_z + b_2\rho_{zz}\ . \tag{28}$$

By substituting Eq. (28) into Eq. (27), we could obtain the simplified form as follows:

$$\begin{aligned} &-c\left(\frac{c\rho_z}{\rho} - \frac{(\rho[pV_{fe}(\rho)+(1-p)V_{be}(\rho)]+b_1\rho_z+b_2\rho_{zz})\rho_z}{\rho^2}\right) + \\ &\left(\frac{\rho[pV_{fe}(\rho)+(1-p)V_{be}(\rho)]+b_1\rho_z+b_2\rho_{zz}}{\rho} - \lambda\Delta\right)\left(\frac{c\rho_z}{\rho} - \right. \\ &\left.\frac{(\rho[pV_{fe}(\rho)+(1-p)V_{be}(\rho)]+b_1\rho_z+b_2\rho_{zz})\rho_z}{\rho^2}\right) = a\left[pV_{fe}(\rho) + (1-p)V_{be}(\rho) - \right. \\ &\left.\frac{\rho[pV_{fe}(\rho)+(1-p)V_{be}(\rho)]+b_1\rho_z+b_2\rho_{zz}}{\rho}\right] + \frac{\lambda\Delta^2}{2}\left(\frac{c\rho_{zz}}{\rho} - \frac{2c\rho_z^2}{\rho^2} - \frac{q\rho_{zz}}{\rho^2} + \frac{q\rho_z^2}{\rho^3}\right). \end{aligned} \tag{29}$$

By equating the coefficients of ρ_z and ρ_{zz} in Eq. (29), we could easily determine the parameters b_1 and b_2 as follows:

$$\begin{aligned} &b_1 = \frac{c}{a}(c + \lambda\Delta) - \frac{1}{a}(2c + \lambda\Delta) + \frac{1}{a}\left[pV_{fe}(\rho) + (1-p)V_{be}(\rho) - v\right]^2. \\ &b_2 = -\frac{\lambda\Delta^2}{2a}\left(c - \left[pV_{fe}(\rho) + (1-p)V_{be}(\rho)\right]\right). \end{aligned} \tag{30}$$

Let us consider $\rho = \rho_h + \hat{\rho}(x,t)$ near the linear stability criteria. In expanding this through using the Taylor expansions and neglecting the higher-order terms of $\hat{\rho}$, we could obtain the following form:

$$\rho\left(pV_{fe}(\rho)+(1-p)V_{be}(\rho)\right)\approx\rho_h\left(pV_{fe}(\rho_h)+(1-p)V_{be}(\rho_h)\right)+\left(\rho\left(pV_{fe}+(1-p)V_{be}\right)\right)_{\rho}\Big|_{\rho=\rho_h}\hat{\rho}+\frac{1}{2}\left(\rho\left(pV_{fe}+(1-p)V_{be}\right)\right)_{\rho\rho}\Big|_{\rho=\rho_h}\hat{\rho}^2. \tag{31}$$

By combining Eq. (31) with Eq. (25) and transforming $\hat{\rho}$ into ρ, we could obtain the following:

$$-c\rho_z+\left[\left(\rho\left(pV_{fe}+(1-p)V_{be}\right)\right)_{\rho}+\left(\rho\left(pV_{fe}+(1-p)V_{be}\right)\right)_{\rho\rho}\rho\right]\rho_z+b_1\rho_{zz}+b_2\rho_{zzz}=0. \tag{32}$$

Following this, we conducted the following variable transformations:

$$U=-\left[\left(\rho\left(pV_{fe}+(1-p)V_{be}\right)\right)_{\rho}+\left(\rho\left(pV_{fe}+(1-p)V_{be}\right)\right)_{\rho\rho}\rho\right],\quad X=mx,\quad T=-mt. \tag{33}$$

After performing the transformation, the standard Korteweg–de Vries (KdV)–Burgers equation was obtained as follows:

$$U_T+UU_x-mb_1U_{xx}-m^2b_2U_{xxx}=0. \tag{34}$$

Therefore, an analytical solution of the standard KdV–Burgers equation is as follows:

$$U=-\frac{3(-mb_1)^2}{25(-m^2b_2)}\left[\begin{matrix}1+2\tanh\left(\pm\frac{-mb_1}{10m^2}\right)\left(X+\frac{6((-mb_1)^2)}{25(-m^2b_2)}T+\varepsilon_0\right)\\+\tanh^2\left(\pm\frac{-mb_1}{10m^2}\right)\left(X+\frac{6((-mb_1)^2)}{25(-m^2b_2)}T+\varepsilon_0\right)\end{matrix}\right]. \tag{35}$$

where ε_0 denotes an arbitrary constant.

5. Numerical simulations

Numerical simulations were conducted using the model alongside the finite difference method, with Eq. (11) discretized as follows:

$$\rho_i^{j+1}=\rho_i^j+\frac{\Delta t}{\Delta x}\rho_i^j\left(v_i^j-v_{i+1}^j\right)+\frac{\Delta t}{\Delta x}v_i^j\left(\rho_{i-1}^j-\rho_i^j\right). \tag{36}$$

(a) If $v_i^j<c_i^j$,

$$v_i^{j+1}=v_i^j-\frac{\Delta t}{\Delta x}\rho_i^j\left(v_i^j-c_i^j\right)\left(v_{i+1}^j-v_i^j\right)+a\Delta t\left[pV_{fe}\left(\rho_i^j\right)+(1-p)V_{be}\left(\rho_{i-1}^j\right)-v_i^j\right]+\frac{\Delta t\,c_i^j\,\Delta}{2(\Delta x)^2}\left(v_{i+1}^j-2v_i^j+v_{i-1}^j\right). \tag{37}$$

(b) If $v_i^j\geq c_i^j$,

$$v_i^{j+1} = v_i^j - \frac{\Delta t}{\Delta x}\rho_i^j\left(v_i^j - c_i^j\right)\left(v_i^j - v_{i-1}^j\right) + a\Delta t\left[pV_{fe}\left(\rho_i^j\right) + (1-p)V_{be}\left(\rho_{i-1}^j\right) - v_i^j\right] + \frac{\Delta t\, c_i^j\, \Delta}{2(\Delta x)^2}\left(v_{i+1}^j - 2v_i^j + v_{i-1}^j\right). \quad (38)$$

where $c_i^j = \frac{\lambda}{\rho_i^j}$

At the initial stage, Herrmann and Kerner [44] introduced the average density ρ_0 as follows:

$$\rho(x,0) = \rho_0 + \Delta\rho_0\left\{\cosh^{-2}\left[\frac{160}{L}\left(x - \frac{5L}{16}\right)\right] - \frac{1}{4}\cosh^{-2}\left[\frac{40}{L}\left(x - \frac{11L}{32}\right)\right]\right\}. \quad (39)$$

where L is the length of the road and ρ_0 and $\Delta\rho_0$ are respectively the initial density and density fluctuation near the equilibrium density.

A periodic boundary condition (cyclic boundary condition) was implemented to execute the simulation, which can be described as follows:

$$\rho(L,t) = \rho(0,t),\ v(L,t) = v(0,t). \quad (40)$$

In this numerical study, we assumed the following parameter settings: $\rho_0 = 0.08$ veh/m (80.0 veh/km), $\rho_m = 0.2$ veh/m (200.0 veh/km), $\Delta\rho_0 = 0.01$ veh/m (10.0 veh/km), $\Delta x = 100$ m, $\Delta t = 1$ s, $a = 0.4$, $\lambda = 0.5$, and $L = 32.2$ km. Here, for case 1, $v_{ff} = 30$ m/s and $v_{bf} = 30$ m/s, whereas for case 2, $v_{ff} = 30$ m/s and $v_{bf} = 15$ m/s.

Fig. 2a and Fig. 3a present spatiotemporal diagrams for the conventional FVD model, whereas Fig. 2b–d and Fig. 3b–d present diagrams for the proposed model. Here, various initial conditions were set for both case 1 and case 2, and the flow field was investigated in terms of a range of 100–10,000 s. Panels (b)–(d) correspond to $p = 0.95$, 0.90, and 0.80, respectively, in both Fig. 2 and Fig. 3. The amplitude of the density fluctuation was significantly alleviated with the proposed model compared with that of the conventional FVD model, and the rate of the fluctuation was gradually mitigated with the decrease in p value. Because of the introduction of the new backward equilibrium velocity function, the "honk" effect could be implemented, having a positive impact in terms of the driver having the capacity to adjust their velocity to the optimal level. In terms of these phenomena, the jamming area of the flow field was found to consistently disperse, with the flow domain shifting to a steady state within a short period of time. The proposed model performed better in case 1 than in case 2, and the subsequent investigations were thus conducted based on case 1 only.

Fig. 4 shows the average velocity profile across the flow field at the initial state and the final state, with the investigation covering a range of 1,000–2,000 s for the initial state and a range of 9,000–10,000 s for the final state. The flow field gradually stabilized according to the time, which is a highly natural tendency, with the stability rate increasing with the decrease in p value. As Fig. 4b–d shows, the vehicles enjoyed a largely steady-state environment at the final state, especially for p = 0.80, whereas an unstable situation emerged for the FVD model at the final state, as shown in Fig. 4a. Meanwhile, Fig. 5 shows the velocity profile of the entire domain on a single time step at 10 and 10,000 s. Here, the enhancement of the flow stability, which increased with the decrease in p value, exhibited a similar tendency as shown in Fig. 4, with Fig. 5a showing the results for the conventional FVD model and Fig. 5b–d those for our proposed model.

Fig. 6 shows the hysteresis loop diagrams for velocity vs. density, with the flow field observed from 9,900 to 10,000 s. For the conventional FVD model, the trajectory loop exhibited a large amplitude, as shown in Fig 6a, with the vehicles encountering a high-level velocity instability. By contrast, as Fig. 6b–d

shows, with our proposed model, the range of the hysteresis loops decreased gradually with the decrease in p value, indicating a smoother traffic flow compared with the conventional FVD model. As such, the numerical results demonstrated good agreement with the theoretical results.

6. Conclusion

In this study, we built a new continuum traffic flow model on the basis of the FVD model, with consideration of the follower honk effect through a new backward equilibrium speed function. The backward equilibrium speed function was improved with the introduction of a positive function, much like with the forward equilibrium function, rather than the negative function used in previous studies. For the effect of this new backward equilibrium speed function, every focal vehicle was alerted to consider their follower vehicle in addition to their preceding vehicle, and although the follower vehicle demanded more space using the horn effect to go forward, the focal vehicle attempted to adjust their velocity to the optimal value. These phenomena inevitably enhanced the stability of the flow field. The efficiency of the proposed model was considerably high compared with that of the conventional FVD model, which was confirmed via the neutral stability analysis. Meanwhile, the nonlinear analysis determined the flow behavior close to the critical point through the KdV–Burgers equation and the attendant wave solution. The numerical results verified the theoretical approach and demonstrated that the new backward equilibrium speed function had a significant impact on stabilizing the flow field.

Acknowledgments

This study was partially supported by the Grant-in-Aid for Scientific Research (KAKENHI) from JSPS (Grant No. JP 19KK0262, JP 20H02314, JP 20K21062) awarded to Professor Tanimoto.

References

1. Ma, G., Ma, M., Liang, S., Wang, Y., Zhang, Y.: An improved car-following model accounting for the time-delayed velocity difference and backward looking effect. Commun. Nonlinear Sci. Numer. Simul. 85, (2020). https://doi.org/10.1016/j.cnsns.2020.105221
2. Md. Anowar Hossain, Tanimoto, J.: A microscopic traffic flow model for sharing information from a vehicle to vehicle by considering system time delay effect. Commun. Nonlinear Sci. Numer. Simul. 85, (2020). https://doi.org/10.1016/j.cnsns.2020.105221
3. Tanimoto, J.: Traffic Flow Analysis Dovetailed with Evolutionary Game Theory. In: Springer 6. pp. 159–182 (2015)
4. Ge, H., Meng, X., Ma, J., Lo, S., Ge, H., Meng, X., Ma, J., Lo, S.: An improved car-following model considering influence of other factors on traffic jam. PhLA. 377, 9–12 (2012). https://doi.org/10.1016/J.PHYSLETA.2012.10.005
5. Ou, H., Tang, T.Q., Zhang, J., Zhou, J.M.: A car-following model accounting for probability distribution. Phys. A Stat. Mech. its Appl. 505, 105–113 (2018). https://doi.org/10.1016/j.physa.2018.03.072
6. Orosz, G., Krauskopf, B., Wilson, R.E.: Bifurcations and multiple traffic jams in a car-following model with reaction-time delay. Phys. D Nonlinear Phenom. 211, 277–293 (2005). https://doi.org/10.1016/j.physd.2005.09.004

7. Guo, L., Zhao, X., Yu, S., Li, X., Shi, Z.: An improved car-following model with multiple preceding cars' velocity fluctuation feedback. Phys. A Stat. Mech. its Appl. 471, 436–444 (2017). https://doi.org/10.1016/j.physa.2016.12.071

8. An, S., Xu, L., Qian, L., Chen, G., Luo, H., Li, F.: Car-following model for autonomous vehicles and mixed traffic flow analysis based on discrete following interval. Phys. A Stat. Mech. its Appl. 560, 125246 (2020). https://doi.org/10.1016/j.physa.2020.125246

9. Jiang, R., Wang, R., Wu, Q.S.: Two-lane totally asymmetric exclusion processes with particle creation and annihilation. Phys. A Stat. Mech. its Appl. 375, 247–256 (2007). https://doi.org/10.1016/j.physa.2006.08.025

10. Peng, G., Lu, W., He, H., Gu, Z.: Nonlinear analysis of a new car-following model accounting for the optimal velocity changes with memory. Commun. Nonlinear Sci. Numer. Simul. 40, 197–205 (2016). https://doi.org/10.1016/j.cnsns.2016.04.024

11. Jiang, R., Wu, Q.S., Zhu, Z.J.: A new continuum model for traffic flow and numerical tests. Transp. Res. Part B Methodol. 36, 405–419 (2002). https://doi.org/10.1016/S0191-2615(01)00010-8

12. Piccoli, B., Tosin, A.: Vehicular Traffic: A Review of Continuum Mathematical Models. In: Encyclopedia of Complexity and Systems Science. pp. 9727–9749. Springer New York (2009)

13. Khoshyaran, M.M., Lebacque, J.P.: Continuum Traffic Flow Modelling: Network Approximation, Flow Approximation. In: Springer Proceedings in Physics. pp. 505–513. Springer Science and Business Media Deutschland GmbH (2020)

14. Nagatani, T.: Thermodynamic theory for the jamming transition in traffic flow. Phys. Rev. E - Stat. Physics, Plasmas, Fluids, Relat. Interdiscip. Top. 58, 4271–4276 (1998). https://doi.org/10.1103/PhysRevE.58.4271

15. Gupta, A.K., Katiyar, V.K.: A new anisotropic continuum model for traffic flow. Phys. A Stat. Mech. its Appl. 368, 551–559 (2006). https://doi.org/10.1016/j.physa.2005.12.036

16. Ngoduy, D., Hoogendoorn, S.P., Liu, R.: Continuum modeling of cooperative traffic flow dynamics. Phys. A Stat. Mech. its Appl. 388, 2705–2716 (2009). https://doi.org/10.1016/j.physa.2009.02.040

17. Chen, T., Shi, X., Wong, Y.D.: A lane-changing risk profile analysis method based on time-series clustering. Phys. A Stat. Mech. its Appl. 565, 125567 (2021). https://doi.org/10.1016/j.physa.2020.125567

18. Benjamin, S.C., Johnson, N.F., Hui, P.M.: Cellular automata models of traffic flow along a highway containing a junction. J. Phys. A. Math. Gen. 29, 3119–3127 (1996). https://doi.org/10.1088/0305-4470/29/12/018

19. Tian, J., Jia, B., Ma, S., Zhu, C., Jiang, R., Ding, Y.X.: Cellular automaton model with dynamical 2D speed-gap relation. Transp. Sci. 51, 807–822 (2017). https://doi.org/10.1287/trsc.2015.0667

20. Zhu, W.X., Zhang, H.M.: Analysis of mixed traffic flow with human-driving and autonomous cars based on car-following model. Phys. A Stat. Mech. its Appl. 496, 274–285 (2018). https://doi.org/10.1016/j.physa.2017.12.103

21. Kala, R., Warwick, K.: Motion planning of autonomous vehicles in a non-autonomous vehicle environment without speed lanes. Eng. Appl. Artif. Intell. 26, 1588–1601 (2013). https://doi.org/10.1016/j.engappai.2013.02.001

22. Li, Z., Li, W., Xu, S., Qian, Y., Sun, J.: Traffic behavior of mixed traffic flow with two kinds of

different self-stabilizing control vehicles. Phys. A Stat. Mech. its Appl. 436, 729–738 (2015). https://doi.org/10.1016/j.physa.2015.05.090

23. Peng, G.: A new lattice model of traffic flow with the consideration of individual difference of anticipation driving behavior. Commun. Nonlinear Sci. Numer. Simul. 18, 2801–2806 (2013). https://doi.org/10.1016/j.cnsns.2013.03.007

24. Li, X., Li, Z., Han, X., Dai, S.: Effect of the optimal velocity function on traffic phase transitions in lattice hydrodynamic models. Commun. Nonlinear Sci. Numer. Simul. 14, 2171–2177 (2009). https://doi.org/10.1016/j.cnsns.2008.06.017

25. Li, Z., Zhang, R., Xu, S., Qian, Y.: Study on the effects of driver's lane-changing aggressiveness on traffic stability from an extended two-lane lattice model. Commun. Nonlinear Sci. Numer. Simul. 24, 52–63 (2015). https://doi.org/10.1016/j.cnsns.2014.12.007

26. Zhang, G., Sun, D. hua, Zhao, M.: Phase transition of a new lattice hydrodynamic model with consideration of on-ramp and off-ramp. Commun. Nonlinear Sci. Numer. Simul. 54, 347–355 (2018). https://doi.org/10.1016/j.cnsns.2017.06.011

27. Zhu, C., Zhong, S., Ma, S.: Two-lane lattice hydrodynamic model considering the empirical lane-changing rate. Commun. Nonlinear Sci. Numer. Simul. 73, 229–243 (2019). https://doi.org/10.1016/j.cnsns.2019.02.010

28. Gupta, A.K., Redhu, P.: Analysis of a modified two-lane lattice model by considering the density difference effect. Commun. Nonlinear Sci. Numer. Simul. 19, 1600–1610 (2014). https://doi.org/10.1016/j.cnsns.2013.09.027

29. Lighthill M.J., W.G.B.: On kinematic waves II. A theory of traffic flow on long crowded roads. Proc. R. Soc. London. Ser. A. Math. Phys. Sci. 229, 317–345 (1955). https://doi.org/10.1098/rspa.1955.0089

30. Lighthill M.J., W.G.B.: On kinematic waves I. Flood movement in long rivers. Proc. R. Soc. London. Ser. A. Math. Phys. Sci. 229, 281–316 (1955). https://doi.org/10.1098/rspa.1955.0088

31. Richards, P.I.: Shock Waves on the Highway. Oper. Res. 4, 42–51 (1956). https://doi.org/10.1287/opre.4.1.42

32. Payne, H.J.: Mathematical Models of Public Systems. Simul. Counc. 1, 51–61 (1971). https://doi.org/10.1098/rspa.1955.0089

33. Bando, M., Hasebe, K., Nakayama, A., Shibata, A., Sugiyama, Y.: Dynamical model of traffic congestion and numerical simulation. Phys. Rev. E. 51, 1035–1042 (1995). https://doi.org/10.1103/PhysRevE.51.1035

34. Helbing, D., Tilch, B.: Generalized force model of traffic dynamics. Phys. Rev. E - Stat. Physics, Plasmas, Fluids, Relat. Interdiscip. Top. 58, 133–138 (1998). https://doi.org/10.1103/PhysRevE.58.133

35. Jiang, R., Wu, Q., Zhu, Z.: Full velocity difference model for a car-following theory. Phys. Rev. E - Stat. Physics, Plasmas, Fluids, Relat. Interdiscip. Top. 64, 4 (2001). https://doi.org/10.1103/PhysRevE.64.017101

36. Nakayama, A., Sugiyama, Y., Hasebe, K.: Effect of looking at the car that follows in an optimal velocity model of traffic flow. Phys. Rev. E - Stat. Physics, Plasmas, Fluids, Relat. Interdiscip. Top. 65, 016112 (2002). https://doi.org/10.1103/PhysRevE.65.016112

37. Hossain, M.A., Kabir, K.M.A., Tanimoto, J.: Improved Car-Following Model Considering Modified Backward Optimal Velocity and Velocity Difference with Backward-Looking Effect. J. Appl. Math. Phys. 09, 242–259 (2021). https://doi.org/10.4236/jamp.2021.92018

38. Kuang, H., Xu, Z.P., Li, X.L., Lo, S.M.: An extended car-following model accounting for the honk effect and numerical tests. Nonlinear Dyn. 87, 149–157 (2017). https://doi.org/10.1007/s11071-016-3032-6

39. Liu, Z., Wang, J., Ge, H., Cheng, R.: KdV-Burgers equation in the modified continuum model considering the "backward looking" effect. Nonlinear Dyn. 91, 2007–2017 (2018). https://doi.org/10.1007/s11071-017-3999-7

40. Chen, C., Cheng, R., Ge, H.: An extended car-following model considering driver's sensory memory and the backward looking effect. Phys. A Stat. Mech. its Appl. 525, 278–289 (2019). https://doi.org/10.1016/j.physa.2019.03.099

41. Wang, Q., Ge, H.: An improved lattice hydrodynamic model accounting for the effect of "backward looking" and flow integral. Phys. A Stat. Mech. its Appl. 513, 438–446 (2019). https://doi.org/10.1016/j.physa.2018.09.025

42. Wang, Z., Ge, H., Cheng, R.: Nonlinear analysis for a modified continuum model considering driver's memory and backward looking effect. Phys. A Stat. Mech. its Appl. 508, 18–27 (2018). https://doi.org/10.1016/j.physa.2018.05.072

43. Jiao, Y., Ge, H., Cheng, R.: Nonlinear analysis for a modified continuum model considering electronic throttle (ET) and backward looking effect. Phys. A Stat. Mech. its Appl. 535, 122362 (2019). https://doi.org/10.1016/j.physa.2019.122362

44. Herrmann, M., Kerner, B.S.: Local cluster effect in different traffic flow models. Phys. A Stat. Mech. its Appl. 255, 163–188 (1998). https://doi.org/10.1016/S0378-4371(98)00102-2

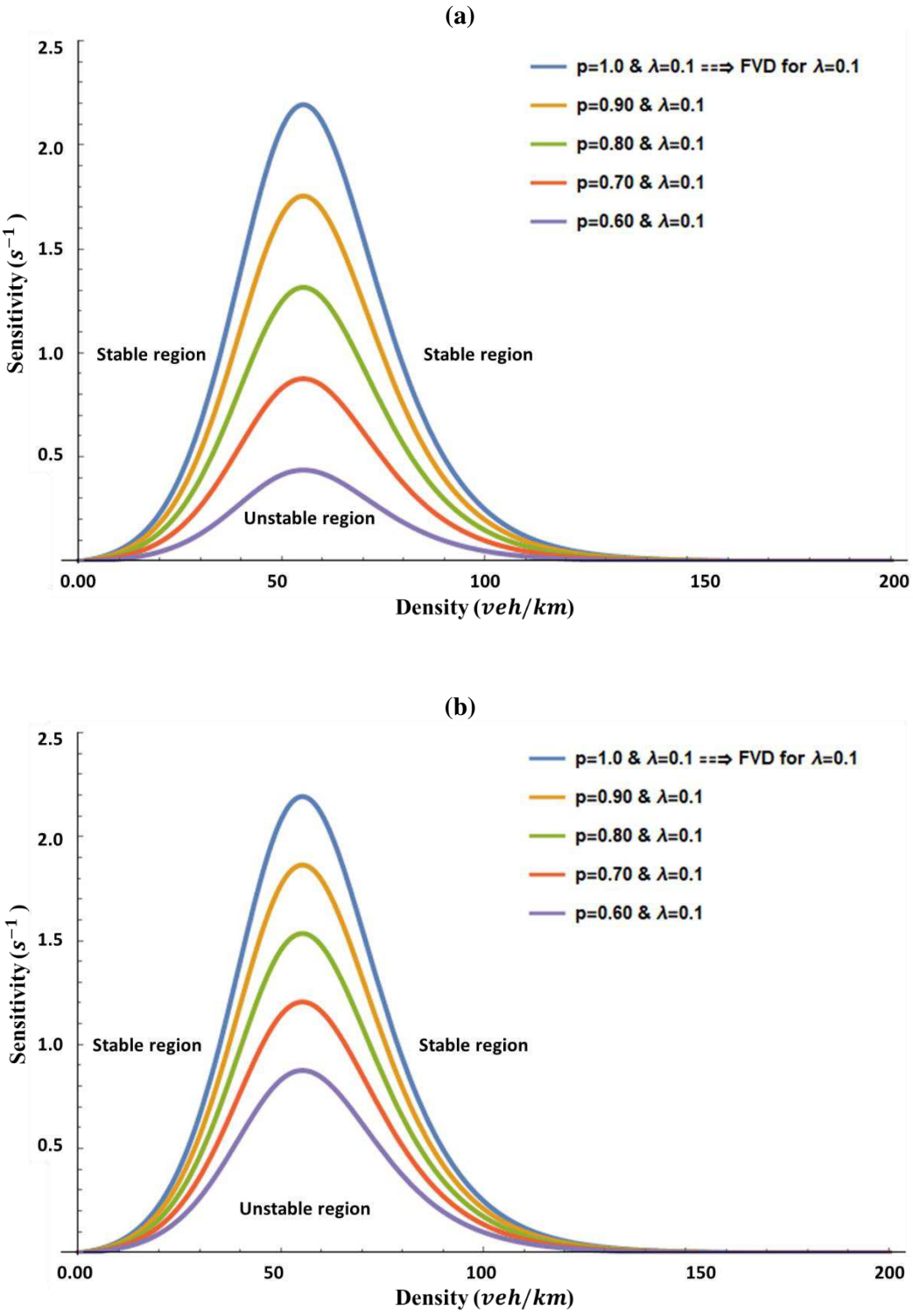

Fig. 1 Neutral stability curves of the model with different p values for (a) $v_{ff} = v_{bf} = 30$ m/s and (b) $v_{ff} = 30$ m/s and $v_{bf} = 15$ m/s.

Case 1

(a) $p = 1.0$ **(b)** $p = 0.95$

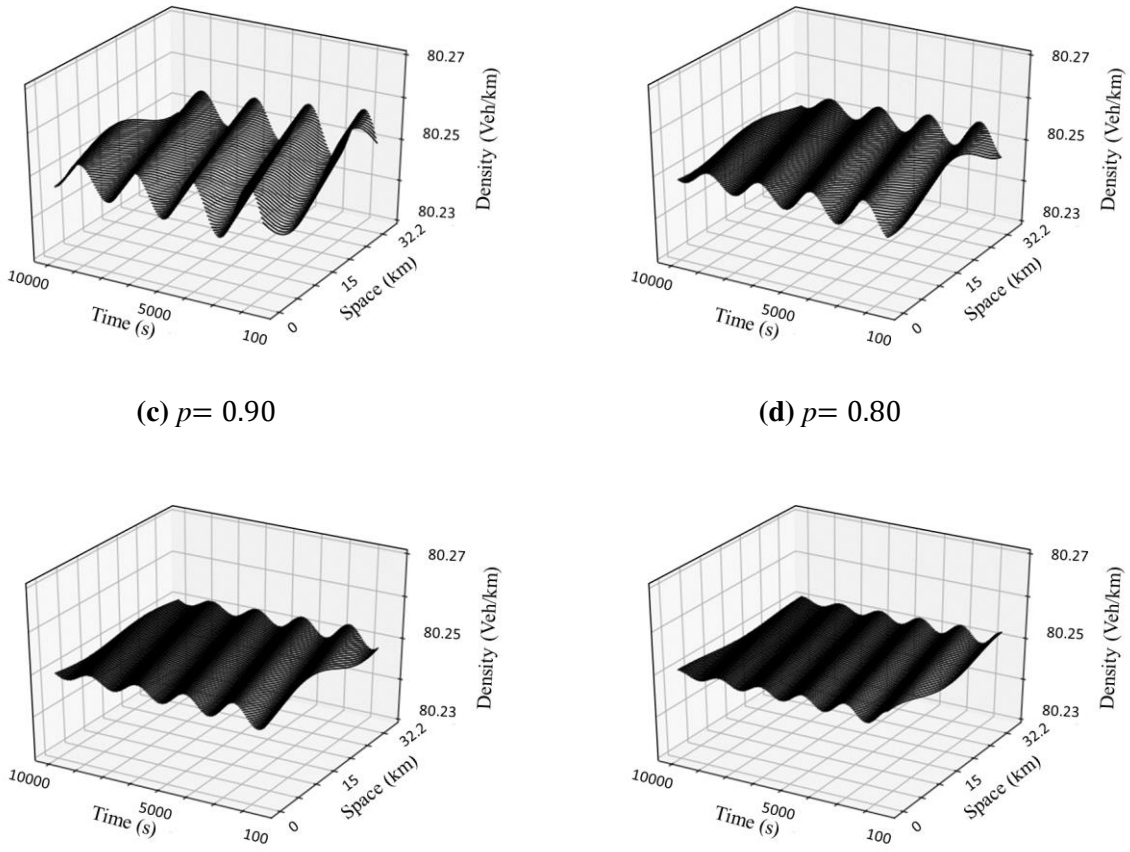

(c) $p = 0.90$ **(d)** $p = 0.80$

Fig. 2 The spatiotemporal diagrams of Time, Space and Density while $v_{ff} = v_{bf} = 30$ m/s for (a) p=1.0, (b) p=0.95, (c) p=0.90 and (d) p=0.80.

Case 2

(a) p= 1.0 **(b)** p= 0.95

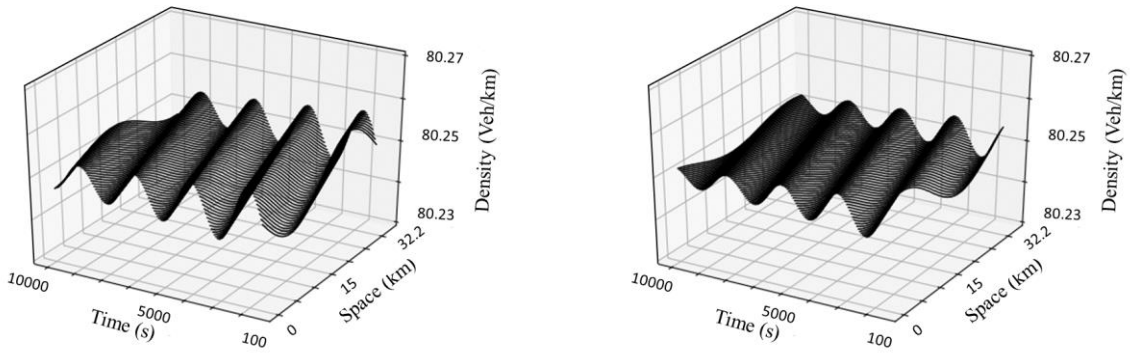

(c) p= 0.90 **(d)** p= 0.80

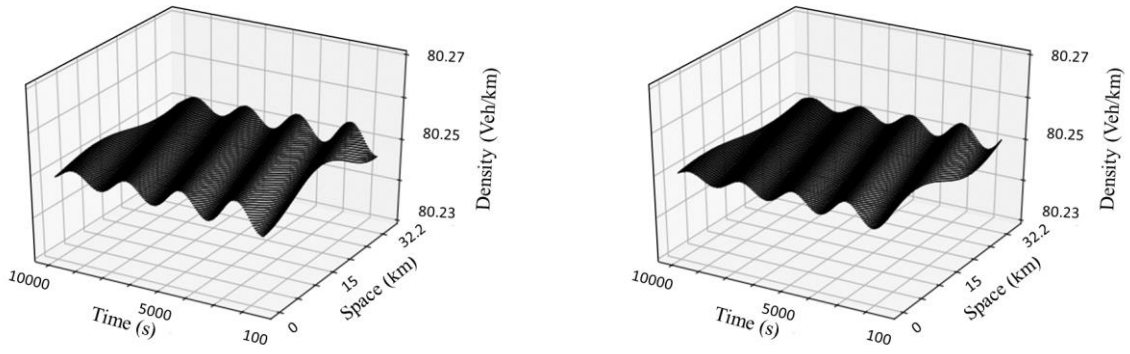

Fig. 3 The spatiotemporal diagrams of Time, Space and Density while $v_{ff} = 30$ m/s and $v_{bf} = 15$ m/s for (a) p=1.0, (b) p=0.95, (c) p=0.90 and (d) p=0.80.

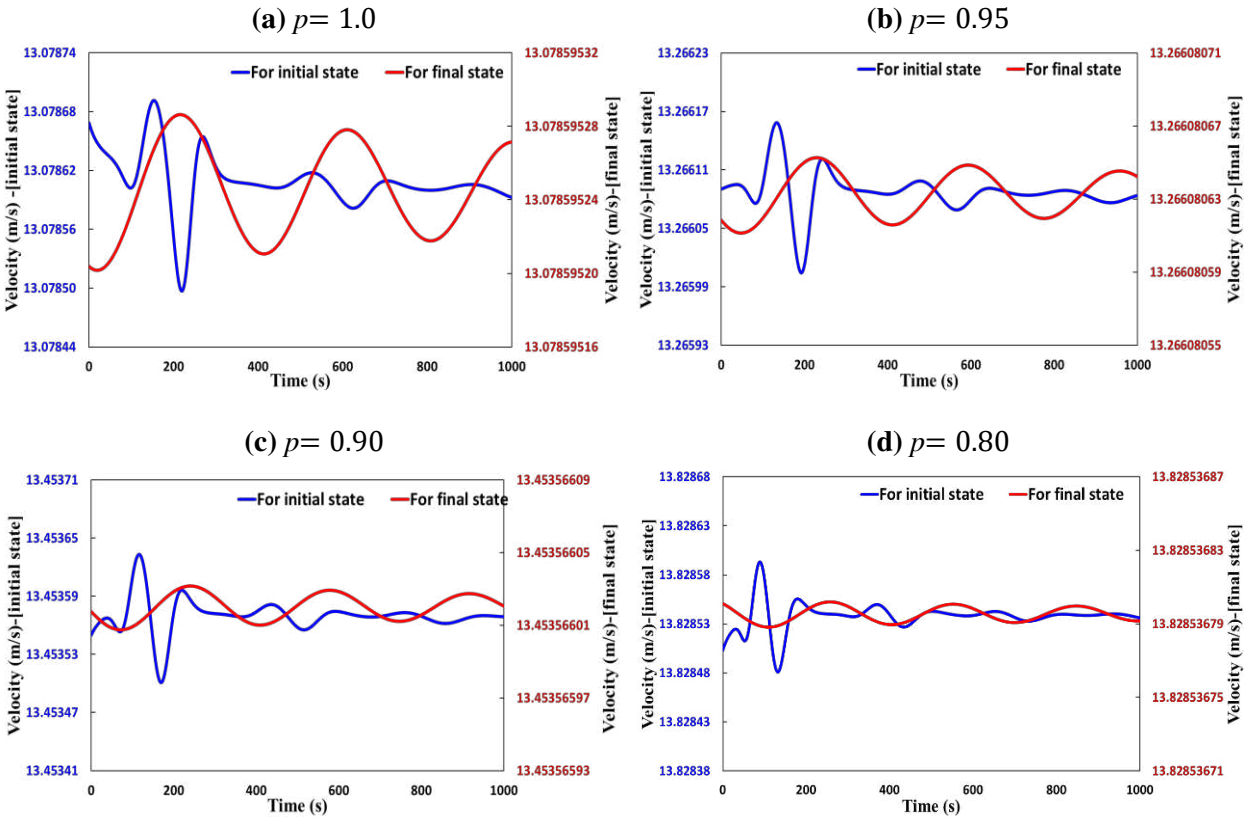

Fig. 4 The velocity profile all over the flow field at initial state and final state for (a) p=1.0, (b) p=0.95, (c) p=0.90 and (d) p=0.80.

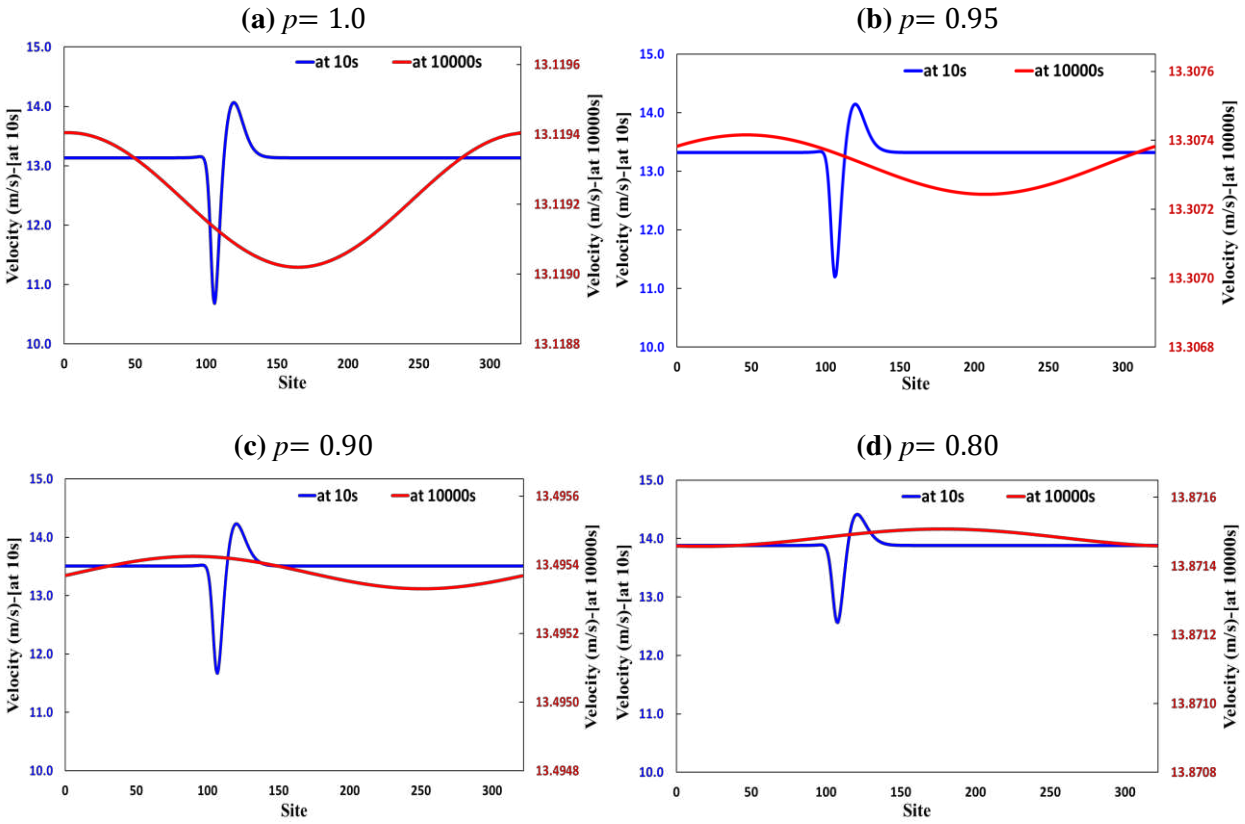

Fig. 5 The velocity profile of the entire domain in a single time step at time 10s and 1000s for (a) p=1.0, (b) p=0.95, (c) p=0.90 and (d) p=0.80

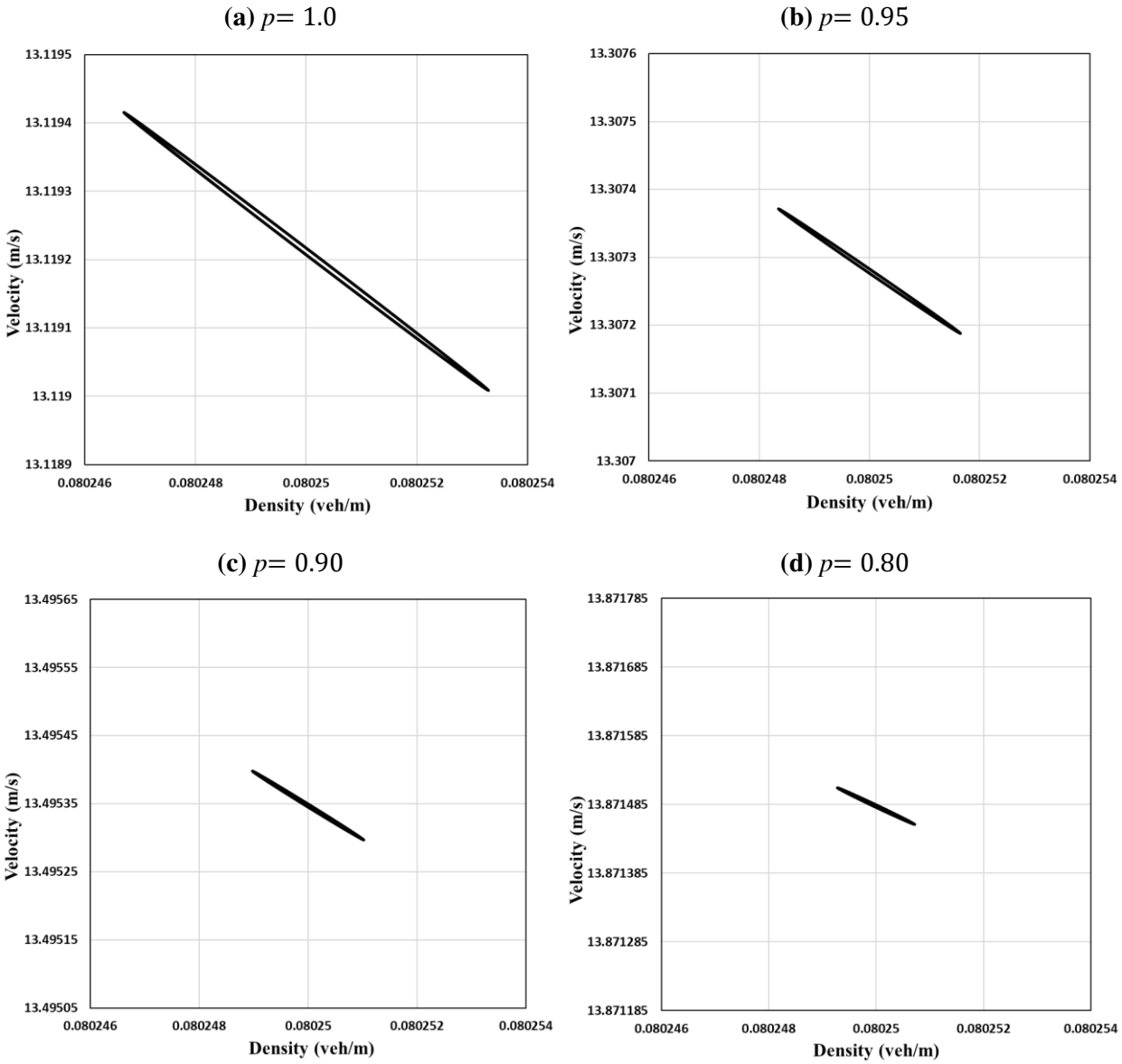

Fig. 6 The hysteresis loop diagrams of velocity vs density for the time steps 9900s to 10000s for (a) p=1.0, (b) p=0.95, (c) p=0.90 and (d) p=0.80.

Figures

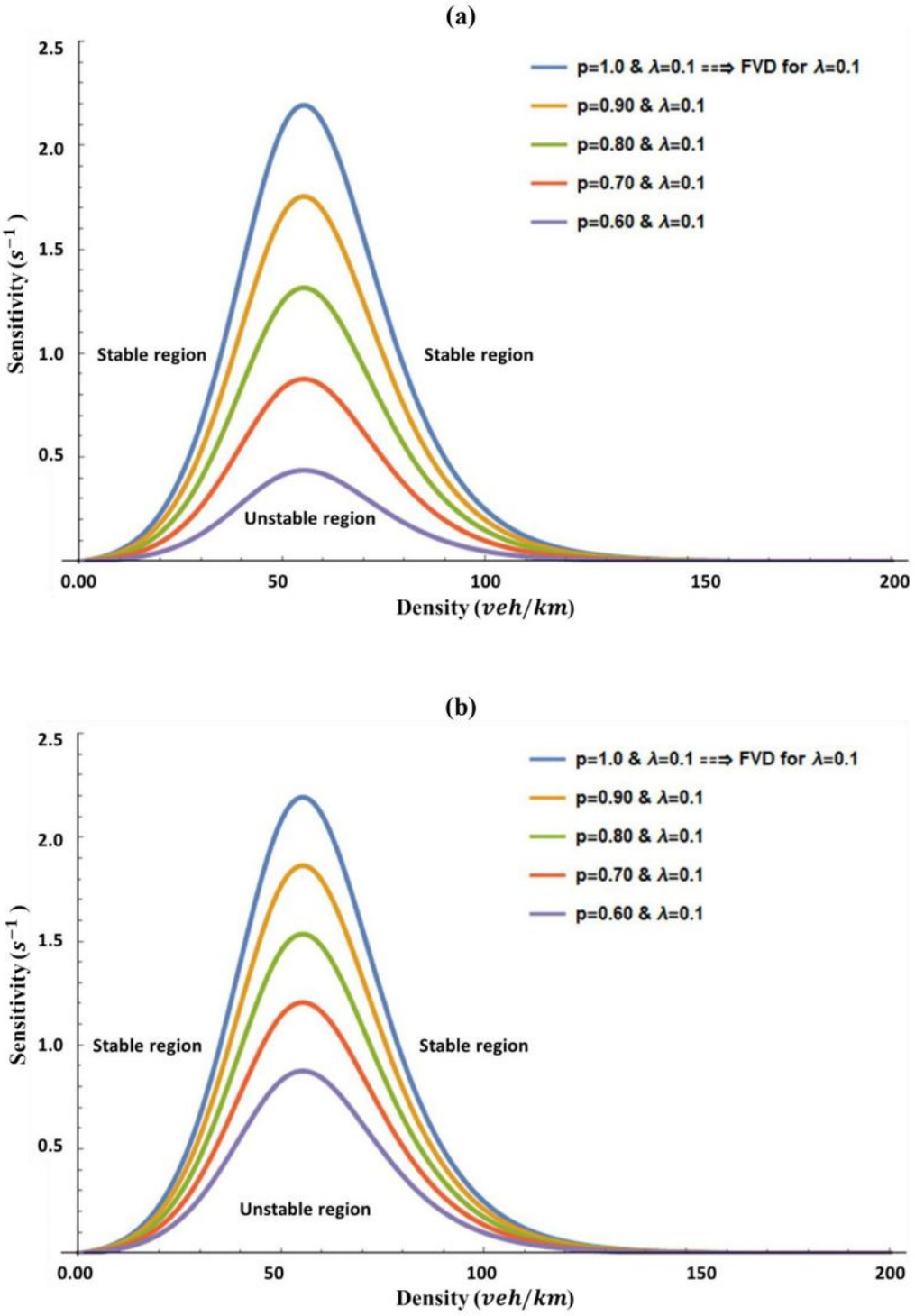

Figure 1

Neutral stability curves of the model with different p values for (a) □□□ = □□□ = 30 m/s and (b) □□□ = 30 m/s and □□□ = 15 m/s.

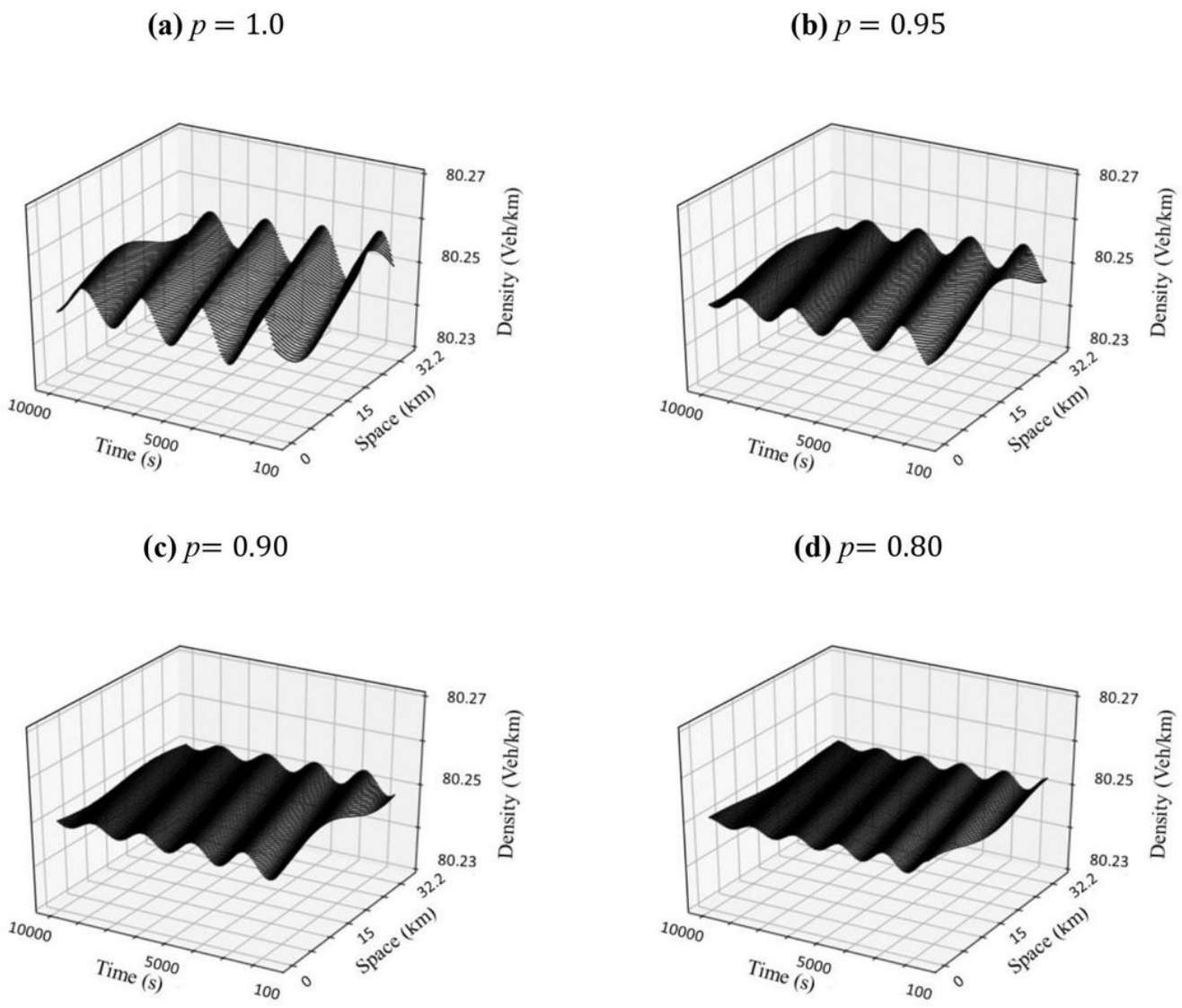

Figure 2

The spatiotemporal diagrams of Time, Space and Density while □□□ = □□□ = 30 m/s for (a) p=1.0, (b) p=0.95, (c) p=0.90 and (d) p=0.80.

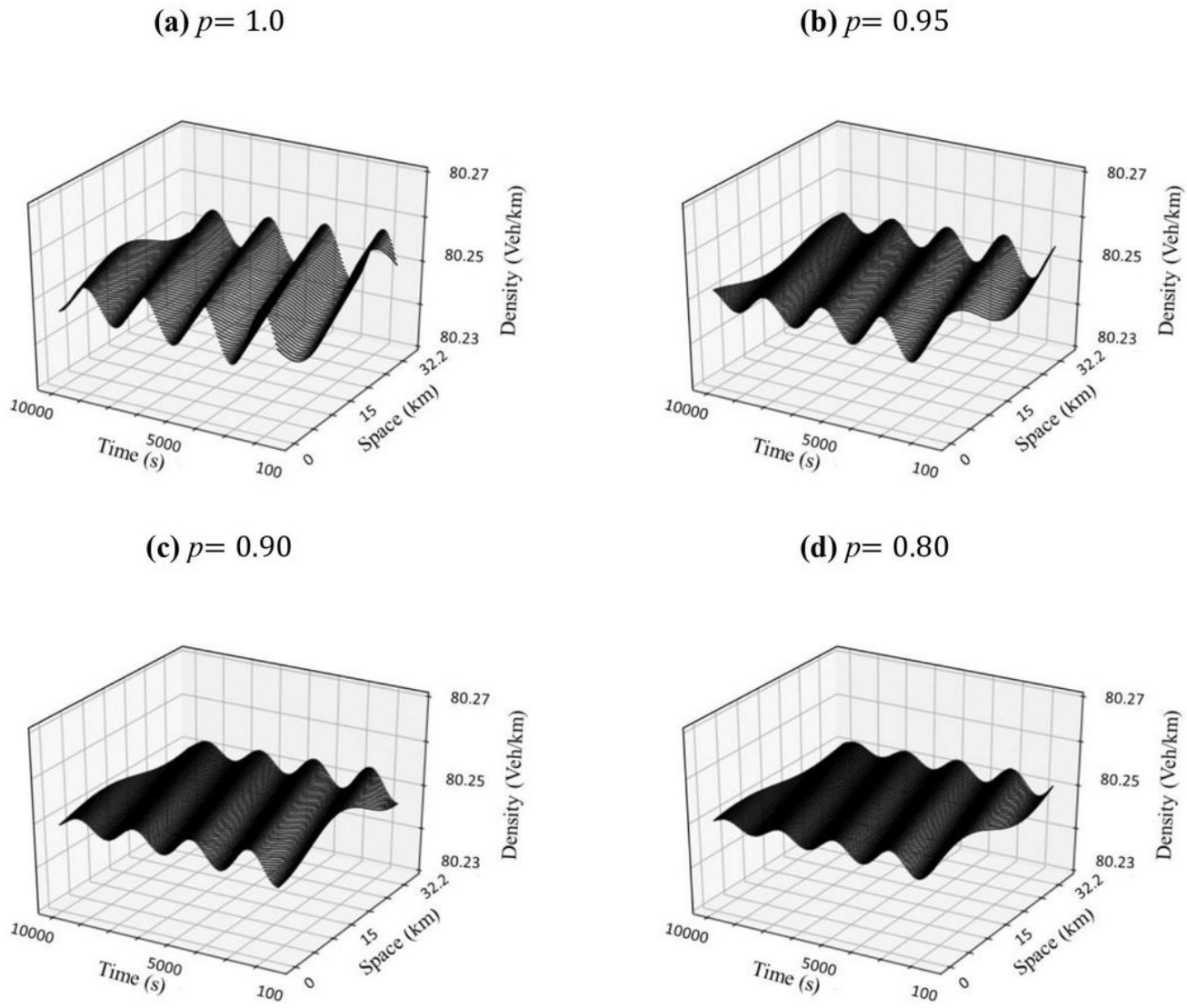

Figure 3

The spatiotemporal diagrams of Time, Space and Density while □□□ = 30 m/s and □□□ = 15 m/s for (a) p=1.0, (b) p=0.95, (c) p=0.90 and (d) p=0.80.

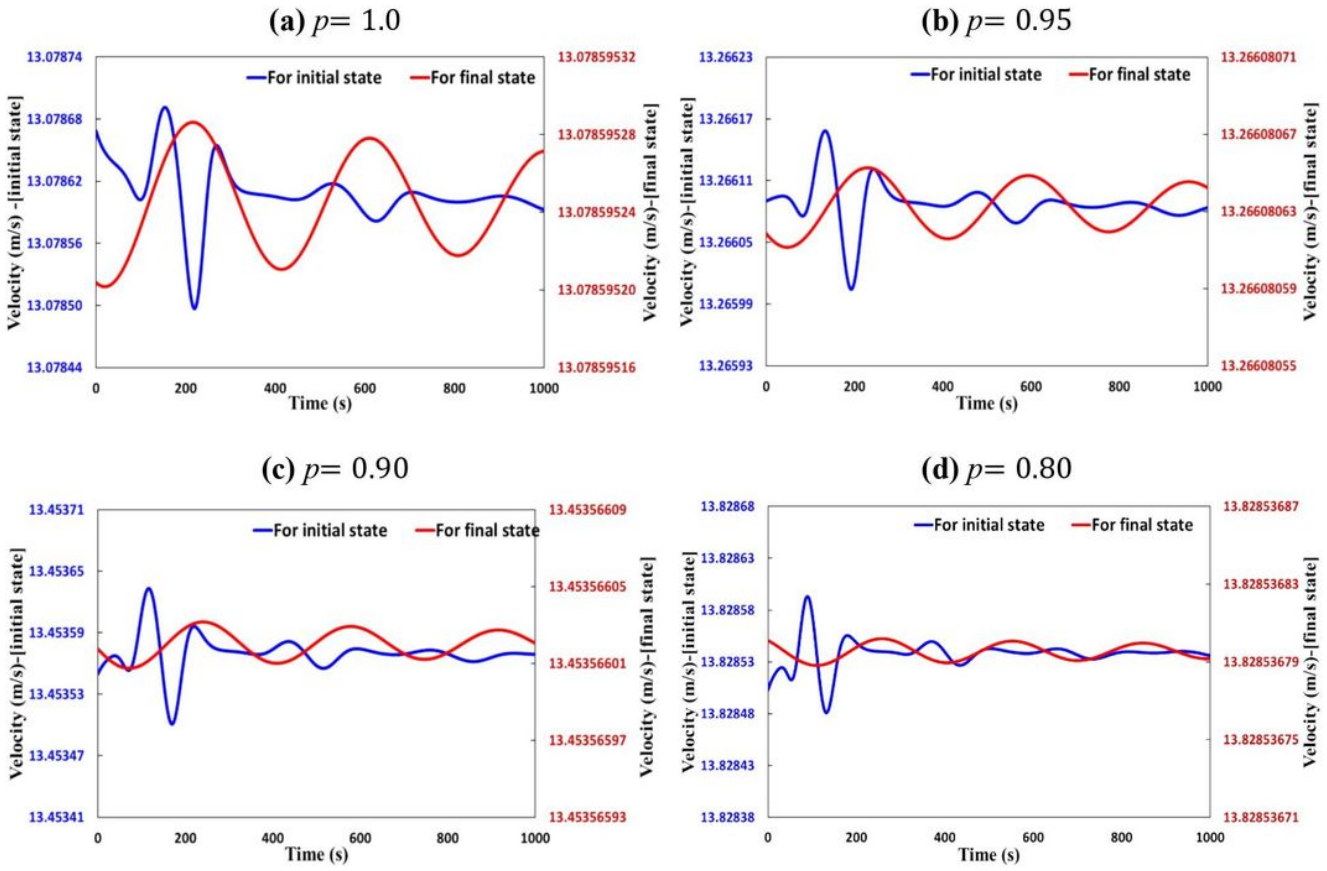

Figure 4

The velocity profile all over the flow field at initial state and final state for (a) p=1.0, (b) p=0.95, (c) p=0.90 and (d) p=0.80.

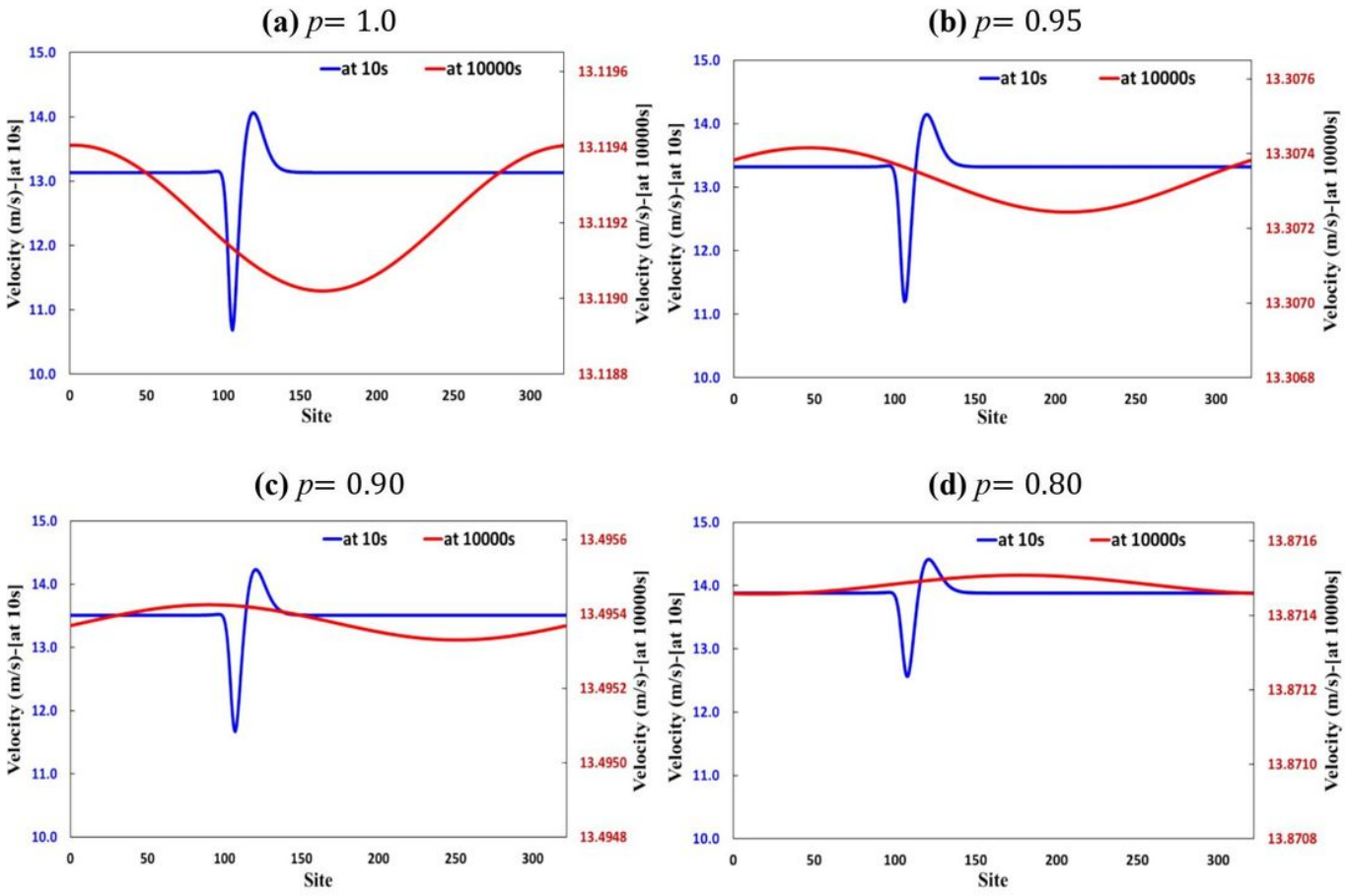

Figure 5

The velocity profile of the entire domain in a single time step at time 10s and 1000s for (a) p=1.0, (b) p=0.95, (c) p=0.90 and (d) p=0.80

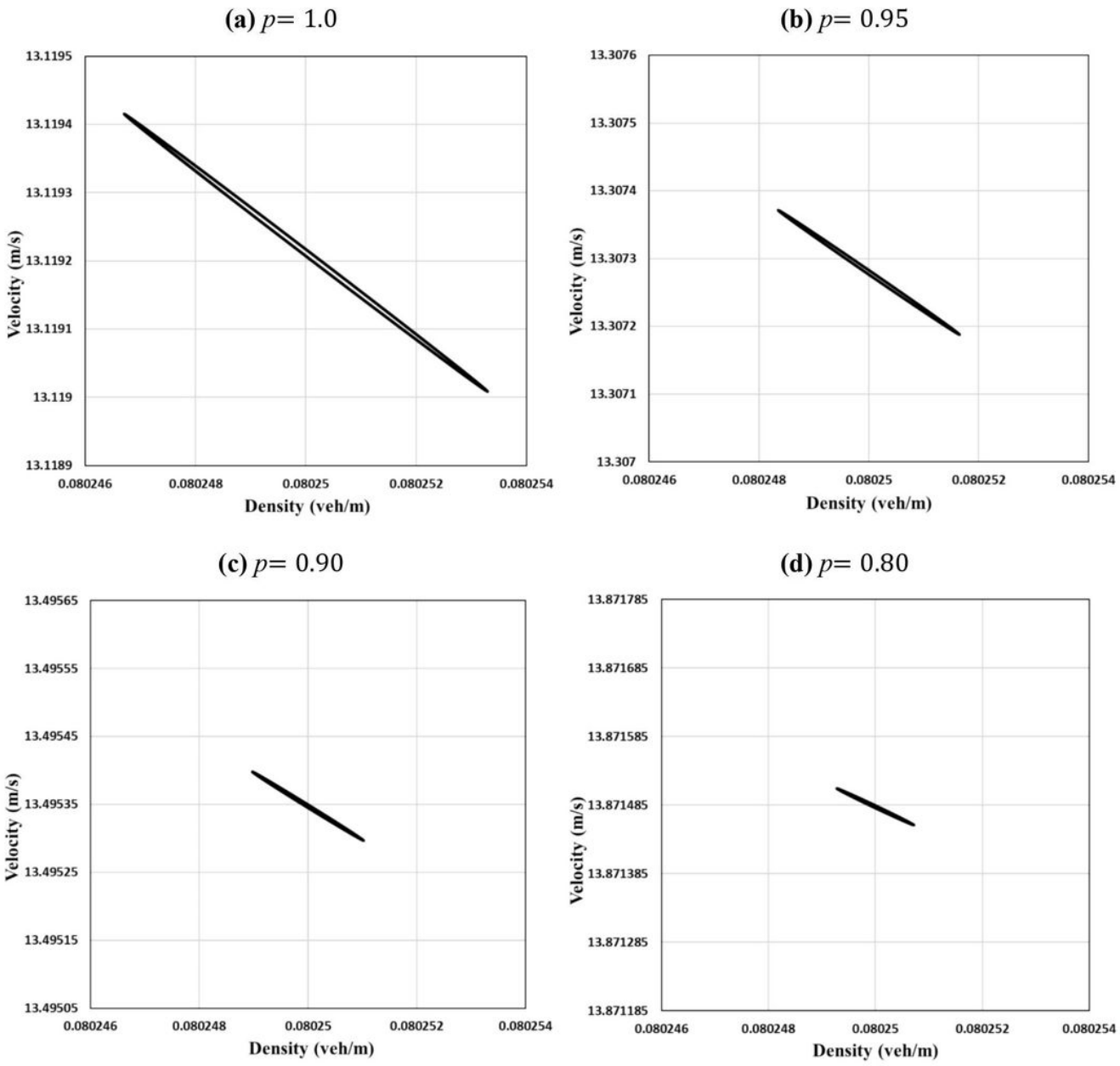

Figure 6

The hysteresis loop diagrams of velocity vs density for the time steps 9900s to 10000s for (a) p=1.0, (b) p=0.95, (c) p=0.90 and (d) p=0.80